View Article Online / Journal Homepage / Table of Contents for this issue
Dynamic Article Links

Polymer Chemistry

Cite this: *Polym. Chem.*, 2012, **3**, 2393

www.rsc.org/polymers

PAPER

Aggregation induced emission enhancement in relation to the secondary structures of poly(γ-benzyl-L-glutamate) containing a fluorescent tetraphenylthiophene moiety†

Shu-Ting Li,[a] Yung-Chih Lin,[a] Shiao-Wei Kuo,[a] Wei-Tsung Chuang[b] and Jin-Long Hong*[a]

Received 12th April 2012, Accepted 8th May 2012
DOI: 10.1039/c2py20221b

Published on 18 June 2012 on http://pubs.rsc.org | doi:10.1039/C2PY20221B
Downloaded by Synchrotron Radiation Library on 21 February 2013

In this study, tetraphenylthiophene (TP) with aggregation-induced emission enhancement (AIEE) property served as the terminal and central fluorophores of poly(γ-benzyl-L-glutamate) (PBLG)-based polymers of TP1PBLG and TP2PBLG, respectively, to probe the relationship between the secondary structure (α-helix) of polypeptides and the AIEE-operative fluorescence (FL). Intermolecular aggregation of the central TP unit in the di-substituted TP2PBLG is sterically blocked by the large α-helical PBLG chains, which leads to the reduced AIEE-oriented FL. In contrast, the terminal TP units in TP1PBLG can easily approach each other to form aggregates with strong FL. Factors (*e.g.* solvent annealing) controlling the fraction of the α-helix chain also vary the corresponding emission intensity. The conformational difference between TP1PBLG and TP2PBLG evaluated from the infrared and the X-ray (wide- and small-angle) diffraction spectra is also used to verify its influence on the AIEE-operative FL behavior.

Introduction

Considerable efforts to investigate polypeptides have been attempted due to their potential applications in various scientific fields and their close relationship to molecular recognition and proteins.[1] The secondary structures of peptide chains play crucial roles in the formation of the well-defined tertiary structure of proteins, therefore, study on the synthetic poly(γ-benzyl-L-glutamate) (PBLG) and its chain conformations in organic solvents illustrates one of the major efforts dedicated previously for the understanding of the complicated protein–protein interactions.

In many organic solvents, PBLG shows various conformation and aggregation structures depending on the solvent.[2] PBLG is dispersed molecularly with the α-helical conformation in *N*,*N*-dimethylformamide (DMF) or *m*-cresol and with the random-coil conformation in dichloroacetic and trifluoroacetic (TFA) acids.[2a–c] The α-helical structures of PBLG form aggregates with an antiparallel side-by-side arrangement[2f,g] in 1,4-dioxane or with a head-to-tail[2a,b,g] arrangement in chloroform, 1,2-dichloroethane and tetrahydrofuran (THF). All these illustrate the versatile conformational possibilities for polypeptide PBLG. As fluorescence (FL) spectroscopy constitutes one of the most powerful tools to study the aggregation of polymers, traditional fluorescent probes such as carbazolyl,[2b] dansyl[2h] and pyrene[2i] (Py) have been chemically incorporated with PBLG to monitor the chain conformations of PBLG in solution. For example, poly(ethylene glycol)-*b*-PBLG has been labeled with Py[2i] and the absence of excimer emission suggested that the Py groups were separated from each other in the self-assembled structure. A study on triblock PBLG–polyfluorene–PBLG copolymers[2j] suggested that formations of rod–rod–rod and coil–rod–coil conformations are dependent on the solvent casting history and the morphological variations resulted in different FL emission and FL decay behaviors. All previous studies suggested that fluorophore-labeled PBLG is a useful methodology to detect the aggregation behavior of the PBLG chain. Traditional fluorophores with coplanar molecular structures emit weakly in the condensed state but in contrast, the non-coplanar silole molecule (1-methyl-1,2,3,4,5-pentaphenylsilole) was found to have strong emission in the aggregated and solid states despite it being non-emissive in the dilute solution.[3a] This interesting character was previously designated as "aggregation-induced emission" (AIE) to emphasize the fact that the originally non-luminescent solution of silole can be tuned to emit strongly when aggregates formed upon nonsolvent inclusion. Since the first discovery of the silole system, several organic and polymeric materials[3b–k] with AIE or AIE enhancement (AIEE) properties have been prepared and well characterized. With chemical structure similar to silole, tetraphenylthiophene (TP) and TP-derived organic and polymeric materials[3i,j] were developed in our lab and their AIE or

[a]*Department of Materials and Optoelectrical Science, National Sun Yat-Sen University, Kaohsiung, 80424, Taiwan. E-mail: jlhong@mail.nsysu.edu.tw; Fax: +886 07 5254099; Tel: +886 07 5252000 ext. 4065*
[b]*National Synchrotron Radiation Research Center, Hsinchu 30076, Taiwan. E-mail: weitsung@nsrrc.org.tw; Fax: +886 03 5783813; Tel: +886 03 5780281 ext. 7125*

† Electronic supplementary information (ESI) available: The ^{1}H NMR, FTIR and MALDI-TOF spectra and DSC thermograms of all organic molecules and polymers. See DOI: 10.1039/c2py20221b

Published on 18 June 2012 on http://pubs.rsc.org | doi:10.1039/C2PY20221B
Downloaded by Synchrotron Radiation Library on 21 February 2013

AIEE-characters were identified. In addition, this TP fluorophore was previously attached to the hydrophilic poly(*N*-isopropyl acrylamide) (PNIPAM)[3k] to result in a TP–PNIPAM polymer, which is capable of forming micelles with intense FL emission from the aggregated hydrophobic TP core. Heating to a temperature above LCST led to the diminished AIEE-operative emission; therefore, the AIEE-operative FL response can be used to locate the LCST.

In contrast to the previous study[2b,h,i] on PBLGs labeled with traditional fluorophores, a novel AIEE-active TP fluorophore was used in this study to incorporate with PBLG and to probe the relationship between the FL response and the secondary structures of peptide. With this aspect, three TP1PBLG(*n*)s ($n = 26$, 15 and 5, Scheme 1) and one TP2PBLG with the TP fluorophore served as the respective terminal and central groups were prepared. It is envisaged that the AIEE-oriented emission should relate to the ease of the molecular approaches (aggregation) of the TP fluorophores, which in turn can be influenced by the geometrical factors conceptually depicted in Scheme 2. Firstly, the intermolecular approaches of the central TP fluorophore of TP2PBLG are more effectively blocked by the two neighboring PBLG chains as compared to the TP fluorophore of TP1PBLG(*n*)s linked only by one PBLG chain. Secondly, the TP fluorophores with a molecular width of ~9 Å can be more effectively separated from other TP units if they are connected to the PBLG chain in a large α-helical (with diameters in the ranges of 15–26 Å[2a–c]) instead of a β-sheet or flexible random coil structure. On the other hand, intimate contacts of the TP fluorophores are possible if the TP fluorophores are connected by PBLG chains in the planar β-sheet or random coil arrangement. With this aspect, three TP1PBLG(*n*)s with different molecular weights (M_ws) were prepared since MW determines the content of the secondary structures on different PBLGs.[2k,l] In addition, experiments (such as adding trifluoroacetic acid (TFA) and solvent annealing) with the capability to alter the content of the secondary structures of PBLGs were also conducted in this study.

All the attempts to change the polypeptide's structure were conducted to vary the degree of aggregation for the TP

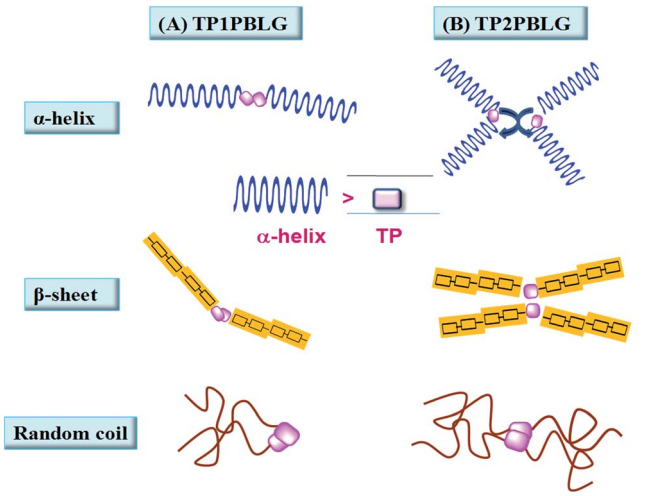

Scheme 2 Mutual approaches between TP fluorophores of the mono- and di-substituted polypeptides with the PBLG chains in α-helix, β-sheet and random-coil structures.

fluorophores, which is supposed to be influential on the observed AIEE-operative emission behavior, embedded in the PBLG chains. Investigations were conducted in both the preparative solution and in the solid states in order to fortify our points. Also, the conformational difference between TP1PBLG(*n*)s and TP2PBLG is evaluated from the corresponding X-ray diffraction study, with the hope to clarify the possible geometrical restrictions on the aggregation tendency of the TP fluorophores in the TP1PBLG(*n*)s and TP2PBLG.

Experimental

Materials

All reagents and chemicals were purchased from Aldrich Chemical Company and used as received. DMSO was refluxed and distilled over CaH_2 under reduced pressure to a flask containing alumina and was used directly after distillation. Compounds of γ-

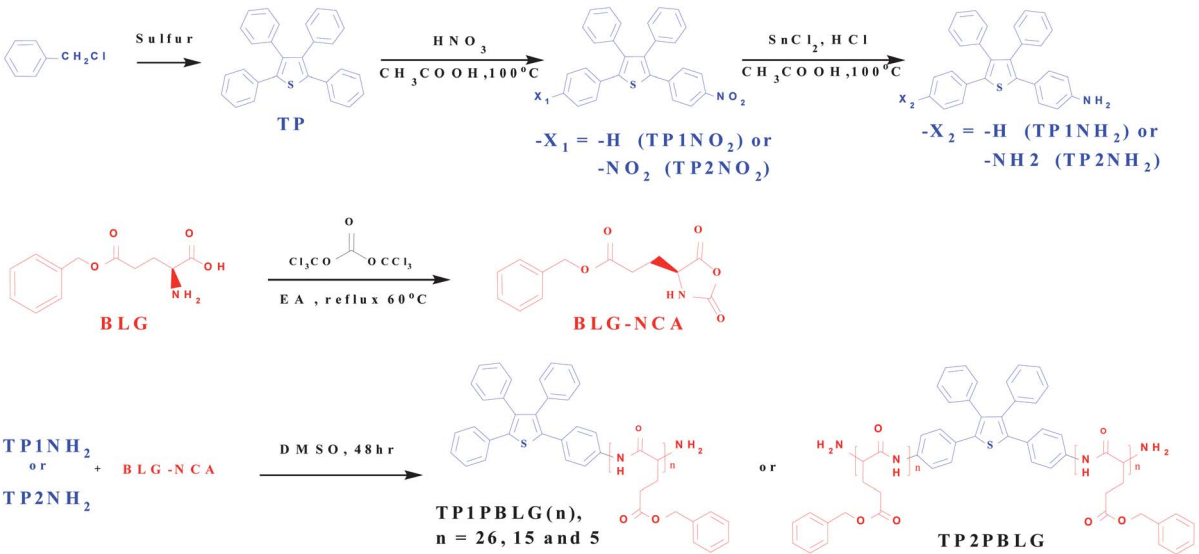

Scheme 1 Preparations of $TP1NH_2$, $TP2NH_2$, and BLG-NCA compounds, and TP1PBLG(*n*) and TP2PBLG polymers.

This journal is © The Royal Society of Chemistry 2012

Published on 18 June 2012 on http://pubs.rsc.org | doi:10.1039/C2PY20221B
Downloaded by Synchrotron Radiation Library on 21 February 2013

benzyl-L-glutamate *N*-carboxyanhydride[4] (BLG-NCA), TP[3j] and $TP1NH_2$[3l] were prepared according to the literature procedures and BLG-NCA was stored at −30 °C before use. Other organic molecules and polymers shown in Scheme 1 were prepared according to the detailed procedures given below.

Synthesis of 2,5-bis(4-nitrophenyl)-3,4-diphenylthiophene ($TP2NO_2$)

A mixture of TP (10 g, 25.74 mmol) and glacial acetic acid (200 mL) was vigorously stirred at 110 °C to result in a homogeneous suspension, to which mixed liquids of glacial acetic acid (20 mL) and concentrated nitric acid (10 mL) were added quickly. After stirring at 100 °C for another 3 h, the yellow suspension was filtered to obtain the crude product. Continuous washing of the crude product with water was performed until the neutral condition (pH = 7) was reached. Column chromatography with hexane eluent yielded the final product (11.21 g; 90% yield). Mp: 220 °C; IR (KBr pellet, cm^{-1}): 3061, 1591, 1515, 1346, 1115, 853, 700 (Fig. S2, ESI†); ^1H NMR (500 MHz, $CDCl_3$): δ 7.95 (d, 4H, H_a), 7.16 (d, 4H, H_b), 7.05–7.13 (m, 8H, H_c, H_d), 6.85 (d, 2H, H_e) (Fig. S1, ESI†); MS *m*/*z*: calcd for $C_{28}H_{18}N_2O_4S$, 478.1; found, 478.9 (M^+). Anal. Calcd for $C_{28}H_{18}N_2O_4S$: C, 70.28; H, 3.79; N, 5.85; O, 13.37; S, 6.7. Found: C, 70.56; H, 3.11; N, 5.76; O, 13.67; S, 6.9%.

Synthesis of 2,5-bis(4-aminophenyl)-3,4-diphenylthiophene ($TP2NH_2$)

$TP2NO_2$ (2.51 g, 5.25 mmol) and glacial acetic acid (25 mL) were charged into a 250 mL round-bottom flask equipped with a reflux condenser, nitrogen inlet and outlet. A solution of stannous chloride dihydrate (12.5 g, 55.4 mmol) in conc. HCl (4 mL) was then added quickly and the whole mixture was heated at 100 °C for 5 h. The mixture was cooled in an ice–salt bath. The solid dihydrochloride salt was filtered and re-dissolved in 15–20 mL of hot water, to which another portion of conc. HCl (3 mL) was added. After cooling to room temperature, the dihydrochloride salt was collected by filtration and dried before re-dissolution in water. A 40% aq. NaOH solution was slowly added to the product solution in an ice–salt bath to the extent of pH = 12. The solid precipitates were then filtered and washed several times with cold water before being dried in a vacuum oven at 40 °C. The crude solid product was recrystallized twice from toluene to yield the white needle-like crystals as the final product (1.75 g, 80% yield). Mp: 283 °C; IR (KBr pellet, cm^{-1}): 3424, 3341, 1624, 1505, 1288, 1184, 824, 703, 528 (Fig. S2, ESI†); ^1H-NMR (500 MHz, DMSO): δ 7.14–7.07 (m, 6H, $H_{f–g}$), 6.92 (d, 4H, H_i), 6.81 (d, 4H, H_h), 6.37 (d, 4H, H_j), 5.18 (s, 4H, H_k) (Fig. 1); MS *m*/*z*: calcd for $C_{28}H_{18}N_2O_4S$, 478.1; found, 478.9 (M^+). Anal. Calcd for $C_{28}H_{18}N_2O_4S$: C, 70.28; H, 3.79; N, 5.85; O, 13.37; S, 6.7. Found: C, 70.56; H, 3.11; N, 5.76; O, 13.67; S, 6.9%.

Preparation of copolymers by ring opening polymerization (ROP)

TP1PBLG(*n*)s and TP2PBLG were prepared by ROP of the BLG monomer initiated by $TP1NH_2$ and $TP2NH_2$, respectively. Preparation of TP2PBLG was used as an example to illustrate its preparation procedures as follows: BLG-NCA (0.5 g, 1.89 mmol) was weighed in a dry-box under argon gas before dissolution by anhydrous DMSO (25 mL) in a flame-dried Schlenk tube. The solution was stirred for 10 min before introducing a solution of $TPNH_2$ (0.02 g, 0.048 mmol) in anhydrous DMSO (5 mL) using a nitrogen purged syringe. After stirring for 40 h at room temperature, the polymer was precipitated from diethyl ether and dried in a vacuum oven (TP2PBLG, 0.37 g, 71% yield). The syntheses of TP1PBLG(*n*)s were operated by the same procedures but with different formulation. TP2PBLG: T_g = 23 °C; IR (KBr pellet, cm^{-1}): 3298, 3044, 2931, 1735, 1653, 1626, 1545; ^1H NMR (500 MHz, CD_2Cl_2): δ 7.84 (broad, 2H, H_d), 7.66 (d, 4H, H_j), 7.30 (broad, 18H, $H_{e–i}$), 5.06 (broad, 4H, H_d), 4.56 (broad, 2H, H_c), 2.44 (broad, 4H, H_b), 2.11–1.88 (broad, 4H, H_a) (Fig. 1). TP1PBLG(26): T_g = 27 °C; IR (KBr pellet, cm^{-1}): 3298, 3044, 2931, 1735, 1653, 1545; ^1H NMR (500 MHz, CD_2Cl_2): δ 7.86 (broad, 2H, H_d), 7.66 (d, 4H, H_j), 7.30 (broad, 18H, $H_{e–i}$), 5.06 (broad, 4H, H_d), 4.56 (broad, 2H, H_c), 2.44 (broad, 4H, H_b), 2.11–1.88 (broad, 4H, H_a) (Fig. S3A, ESI†). TP1PBLG(15): T_g = 26 °C; IR (KBr pellet, cm^{-1}): 3298, 3044, 2931, 1735, 1653, 1625, 1545; ^1H NMR (500 MHz, CD_2Cl_2): δ 8.06–7.81 (broad, 2H, H_d), 7.66 (d, 4H, H_j), 7.30 (broad, 18H, $H_{e–i}$), 5.06 (broad, 4H, H_d), 4.74–4.14 (broad, 2H, H_c), 2.44 (broad, 4H, H_b), 2.11–1.88 (broad, 4H, H_a) (Fig. S3B, ESI†). TP1PBLG(5): T_g = 24 °C; IR (KBr pellet, cm^{-1}): 3298, 3044, 2931, 1735, 1653, 1626, 1545; ^1H NMR (500 MHz, CD_2Cl_2): δ 7.86 (broad, 2H, H_d), 7.66 (d, 4H, H_j), 7.30 (broad, 18H, $H_{e–i}$), 5.06 (broad, 4H, H_d), 4.61 (broad, 2H, H_c), 2.47 (broad, 4H, H_b), 2.11–1.88 (broad, 4H, H_a) (Fig. S3C, ESI†).

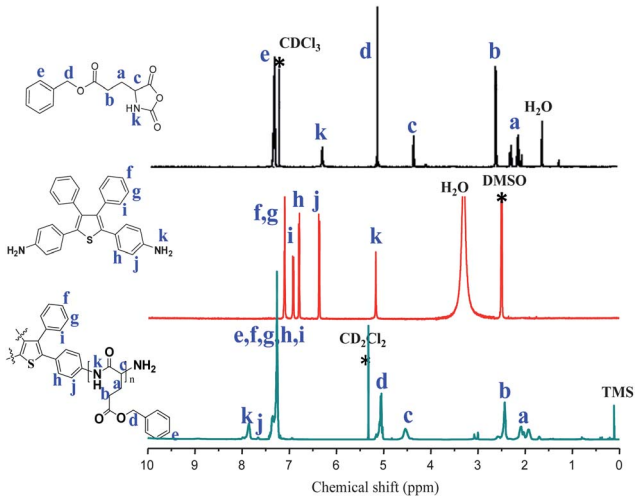

Fig. 1 ^1H NMR spectra of BLG-NCA, $TP2NH_2$ and TP2PBLG (CD_2Cl_2 + 15 v% TFA).

Measurements

^1H NMR spectra were recorded at room temperature using a Bruker AM 500 (500 MHz) spectrometer with tetramethylsilane (TMS) as the external standard. Differential scanning calorimetry (DSC) was performed using a TA-Q20 instrument operated at a scan rate of 10 °C min^{-1} over a temperature range of −70 to 180 °C under a N_2 atmosphere. FTIR spectra were recorded from a Bruker Tensor 27 FTIR spectrophotometer; 32 scans were collected at a spectral resolution of 1 cm^{-1}. The solid

Published on 18 June 2012 on http://pubs.rsc.org | doi:10.1039/C2PY20221B
Downloaded by Synchrotron Radiation Library on 21 February 2013

polymer powders were mixed with KBr before being pressed to make pellets for measurement. Solutions of polymers with predetermined concentrations were placed in a CaF_2 cell for spectral analysis. Mass spectra were obtained from a Bruker Daltonics Autoflex III MALDI-TOF mass spectrometer and operated by the following voltage parameters: ion source 1, 19.06 kV; ion source 2, 16.61 kV; lens, 8.78 kV; reflector 1, 21.08 kV; reflector 2, 9.73 kV. A wide-angle X-ray diffraction (WAXD) pattern was obscured from a Siemens D5000 X-ray diffractometer with a source of Cu Kα ($\lambda = 0.154$ nm) radiation at 40 kV and 30 mA. Diffraction patterns were collected with a scan rate of 3 s per 0.1° in the 2θ ranges of 2–40°. Small-angle X-ray scattering (SAXS) experiments were performed at the SWAXS endstation of the BL17B3 beamline of the Taiwan light source in the National Synchrotron Radiation Research Center (NSRRC); the X-ray beam had a diameter of 0.5 mm and a wavelength (λ) of 0.124 nm. The blend samples (thickness: 1 mm) were sealed between two thin Kapton windows (thickness: 80 mm) and analyzed at room temperature. Grazing-incidence wide-angle X-ray diffraction (GIWAXD) measurement was performed at the BL13A1 SAXS endstation, of the NSRRC, Taiwan. The X-ray beam had a diameter of 0.5 mm and a wavelength (λ) of 0.103 nm. A Mar165 CCD X-ray detector was used to collect the GIWAXD pattern and the sample-to-detector distance was 0.32 m. The angle of incidence was 0.1°. A solution of TP2PBLG in THF was dropped on a 3×3.5 cm^2 silicon substrate and during the solvent evaporation step, a unidirectional shearing force was applied to obtain the oriented film for analysis. PL was obtained from a LabGuide X350 fluorescence spectrophotometer using a 450 W Xe lamp as the continuous light source. UV-vis absorption spectra were recorded with an Ocean Optics DT 1000 CE 376 spectrophotometer. A small quartz cell with dimensions $0.2 \times 1.0 \times 4.5$ cm^3 was used to accommodate the solution sample.

Results and discussion

As illustrated in Scheme 1, polymers of TP1PBLG(n) and TP2PBLG with single and two PBLG chains tethered to an AIEE-active TP fluorophore were prepared by the ring-opening polymerizations (ROPs) of the BLG-NCA monomer initiated by the mono- and the di-amino functionalized $TP1NH_2$ and $TP2NH_2$ initiators, respectively. Both of the $TP1NH_2$ and $TP2NH_2$ initiators were synthesized by a two-step reaction process starting from nitration of TP to generate nitro groups (in $TP1NO_2$ and $TP2NO_2$) followed by the subsequent reduction by $SnCl_2$. Successful polymer preparation can be demonstrated from the related FTIR and ^{1}H NMR spectra. Primarily, the FTIR spectra (Fig. S2, ESI†) indicate that the anhydride stretching (–C(=O)–O–C(=O) at 1849 cm^{-1}) band of the BLG-NCA monomer disappeared and instead the ester and amide stretching (1500–1750 cm^{-1}) bands emerged in the spectrum of TP2PBLG. The ^{1}H NMR spectra of $TP2NH_2$ and TP2PBLG were also used to demonstrate the success of polymerization, as illustrated in Fig. 1, the sharp aromatic resonances (protons **f–j** in Fig. 1) of $TP2NH_2$ in the range of 6.4–7.1 ppm were further downshifted to 7.3–7.6 ppm once incorporated with PBLG chains and became indistinguishable from the aromatic resonance (protons **e**) of the phenyl side groups in TP2PBLG. Here, the integration ratio between aromatic protons **e–j** and methylene proton **d** can be used to calculate the number-average molecular weight ($M_n = 4230$ g mol^{-1}, Table 1) of TP2PBLG, which is well correlated with the value (4240 g mol^{-1}) obtained from the MALDI-TOF mass spectroscopy (Fig. S4D, ESI†). As indicated in Table 1, the resultant MW values of all polymers determined from the ^{1}H NMR and the MALDI-TOF mass spectra are related to each other reasonably. The resultant degree of polymerization (n) of the mono-substituted TP1PBLG(n)s refers to the number of the repeated units calculated from the ^{1}H NMR spectra. The di-substituted TP2PBLG has a total n value of 17, which is lower than that of TP1PBLG(26) but slightly higher than that of TP1PBLG(15).

Table 1 Polymer MW values evaluated from ^{1}H NMR and MALDI-TOF mass spectra[a]

Polymer	From ^{1}H NMR	From MALDI-TOF
TP1PBLG(26)	$M_n = 6160$ ($n = 26$)	$M_n = 6340$ ($n = 27$), $M_w = 6610$, PDI = 1.04
TP1PBLG(15)	$M_n = 3710$ ($n = 15$)	$M_n = 4200$ ($n = 17$), $M_w = 4810$, PDI =1.15
TP1PBLG(5)	$M_n = 1520$ ($n = 5$)	$M_n = 1610$ ($n = 6$), $M_w = 1650$, PDI =1.02
TP2PBLG	$M_n = 4230$ ($n = 17$)	$M_n = 4240$ ($n = 9$), $M_w = 4340$, PDI = 1.02

[a] M_n from ^{1}H NMR was calculated from the integration ratio between aromatic protons ($H_e \approx H_j$) and protons H_d (*cf.* Fig. 1 and S3, ESI†); n refers to the degree of polymerization of PBLG polymers and in the case of TP2PBLG, it refers to the total units incorporated in the two PBLG chains per TP2PBLG.

Solution PL emission study

The AIEE-effect of polymeric TP1PBLG(26), (15) and (5) was primarily evaluated from the solution FL spectra in the solvent–nonsolvent pair of THF–water mixtures. With the bulky TP terminal group, all TP1PBLG(n)s are soluble in THF. With the inclusion of nonsolvent water, aggregates formed as evidenced by the turbid appearance of the mixture solutions. As shown in Fig. 2A–C, all dilute (10^{-5} M, relative to TP fluorophore) solutions of TP1PBLG(n)s in THF are weak in emission. From the 10 to 70 vol% water solutions, the resultant emission intensities continuously grow until the sudden emission reductions for all the 90 vol% water solutions. The unexpected emission reductions for the 90 vol% water solutions are due to the precipitations of the TP1PBLG(n)s in solutions containing a majority of non-solvent water. Here, the two discernible, overlapped emission bands in the short- and long-wavelength regions correspond to the monomer (at 440 nm) and the aggregated (at 488 nm) emissions, respectively. The observed emission intensifications are attributed to the gradually enlarged aggregate emissions, which indicate that the developing aggregation is the key leading to the operative AIEE effect and the resultant emission intensification. Complete blockage of the TP fluorophores from intermolecular approaches is therefore inaccessible for the mono-substituted TP1PBLG(n) polymers. Despite the potential AIEE feature, a dilute solution of TP2PBLG may not emit strongly if all the inherent TP fluorophores are well isolated by the neighboring PBLG chains in the large α-helical structure according to the concept depicted in Scheme 1. Nevertheless, a solution of

This journal is © The Royal Society of Chemistry 2012

Downloaded by Synchrotron Radiation Library on 21 February 2013
Published on 18 June 2012 on http://pubs.rsc.org | doi:10.1039/C2PY20221B

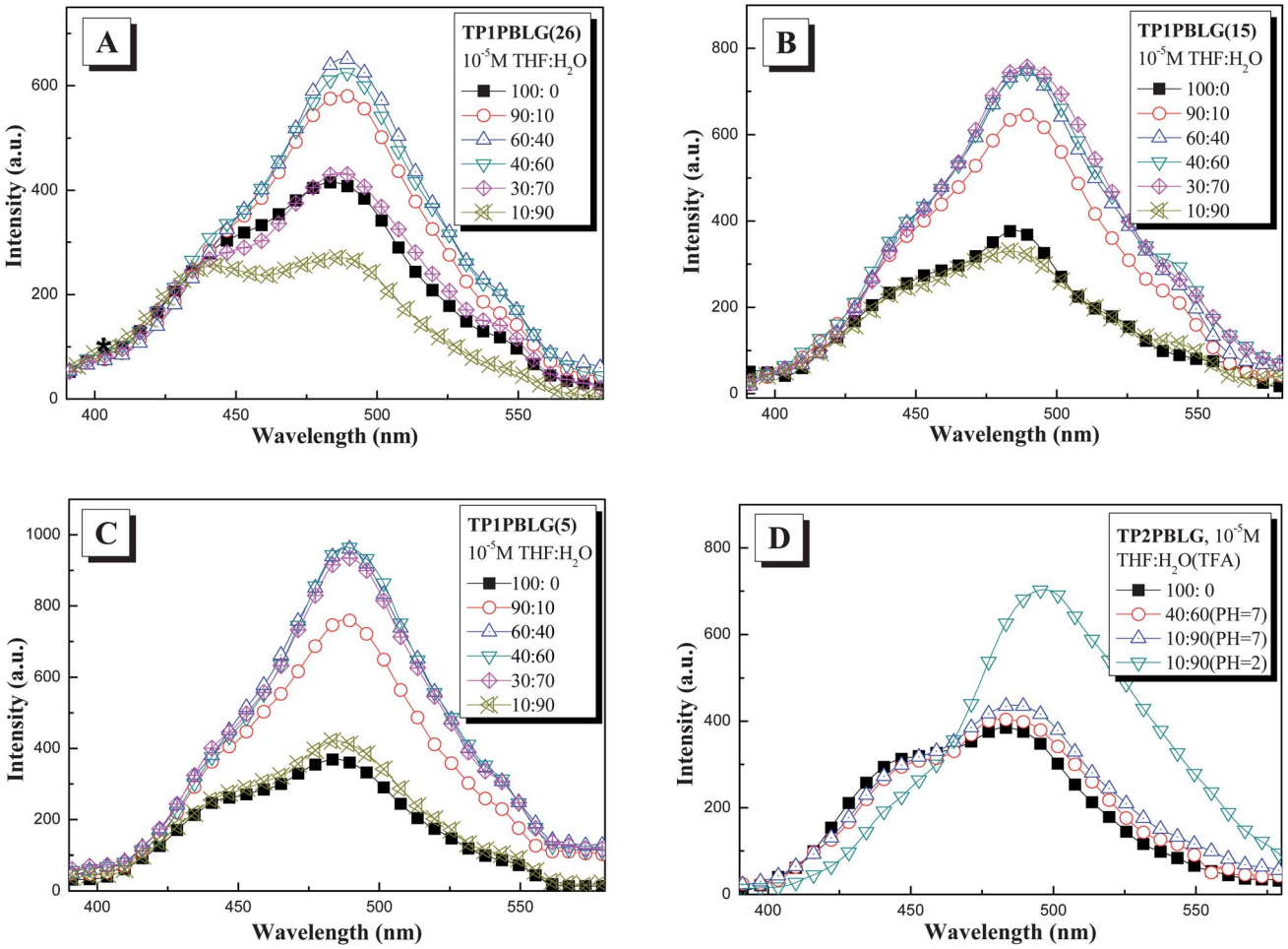

Fig. 2 The solution FL emission spectra of (A) TP1PBLG(26), (B) TP1PBLG(15) and (C) TP1PBLG(5) in THF–water mixtures of varied volume fractions and (D) TP2PBLG in THF–water mixtures with and without the addition of TFA (polymer concentration: 10^{-5} M; λ_{ex} = 350 nm).

TP2PBLG in THF (Fig. 2D) still emitted with a large aggregate emission band located at a longer wavelength of 488 nm as compared to the discernible monomer emission at 440 nm. Therefore, intermolecular approaches of the TP fluorophores in TP2PBLG are still possible and this result may refer to the existence of a β-sheet or random coil structure in the corresponding PBLG chains. As illustrated in Fig. 2D, inclusion of water (with THF–H_2O v/v = 40/60 and 10/90) resulted in little emission variations, which indicates that the steric restrictions from the two PBLG chains are large enough to prevent further aggregation of TP fluorophores; at this moment, the little perturbation on chain conformation during the aggregation process may be due to most of the chain segments being in the large, rigid α-helix structure. Since the α-helical structure of PBLG can be disintegrated by adding trifluoroacetic acid (TFA),[2d] the FL response toward TFA addition was therefore conducted on a solution of TP2PBLG in THF–H_2O (v/v = 10/90). By adding TFA until pH = 2, we observed a large intensity jump in the red-shifted aggregate emission. Helix–coil transformation promoted by TFA will help the aggregation of the central TP fluorophores since according to Scheme 1 the intermolecular approaches among the TP fluorophores vicinal to the random-coil chain are possible. In this case, further aggregation caused by TFA addition may force the TP fluorophores to adopt a more coplanar geometry, which leads to the observed bathochromic shift of the aggregate emission compared to those observed in the neutral solutions.

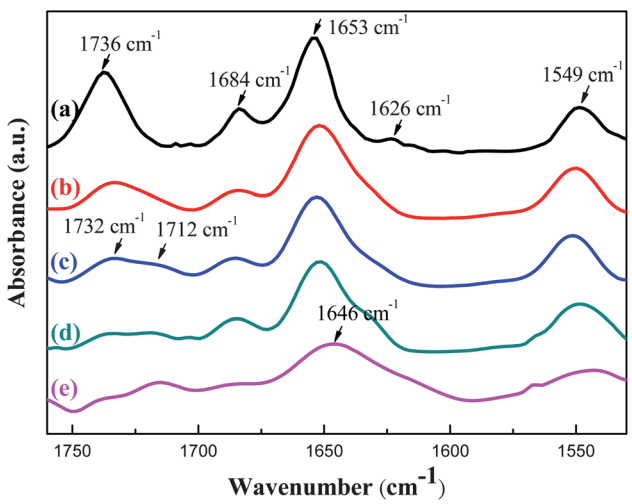

Fig. 3 Solution FTIR spectra of TP2PBLG in THF containing different amounts of TFA. (a) 0 vol% TFA; (b) 0.5 vol% TFA; (c) 1 vol% TFA; (d) 2 vol% TFA and (e) 5 vol% TFA (polymer concentration = 10^{-4} M).

Published on 18 June 2012 on http://pubs.rsc.org | doi:10.1039/C2PY20221B
Downloaded by Synchrotron Radiation Library on 21 February 2013

The effect of TFA addition on the TP2PBLG chain can be evaluated from the corresponding solution FTIR spectra. To attain resolvable intensity, FTIR spectra were thereby taken at a higher concentration of 10^{-4} M instead of 10^{-5} M used in the FL emission study. Solution FTIR spectra of TP2PBLG(*n*) in Fig. 3 suggest that the amide I band at 1653 cm^{-1} is characteristic of the α-helical secondary structure and the amide I bands located at 1626 and 1684 cm^{-1} come from β-sheets in parallel and antiparallel arrangements, respectively, while for a random coil the corresponding band appears at 1646 cm^{-1}.[2m] In addition, the free C═O unit of the side chain group of PBLG provides a signal at 1736 cm^{-1}. Before adding TFA, both the α-helical and β-sheet structures are present in the TP-centered polymer. The introduction of TFA caused an extra shoulder peak at 1712 cm^{-1}, which is due to the hydrogen-bonded (H-bonded) ester carbonyl group, besides the original free ester carbonyl band at 1736 cm^{-1}.

As the H-bonded carbonyl stretching band emerged at a time before a drastic change in the peak (at 1653 cm^{-1}) associated with the α-helical structure occurred, association of the TFA acid with the side group of TP2PBLG should take place prior to the backbone helix–coil transition. With increasing amounts of TFA additives in the solutions, formation of a random coil structure in the later isotopic phase was evidenced by the amide I band at 1646 cm^{-1}, the characteristic vibrational frequency[2n] previously assigned for the random coil conformation. Before TFA addition, the TP fluorophores separated by the α-helical chains emitted weakly but after helix–coil transformation, the inherent TP fluorophores connected by more flexible random coil chains contacted each other easily, which promoted the AIEE-operative emission observed in Fig. 2D.

Secondary structure in relation to the AIEE-effect in the solid state

All solid polymer films cast from the corresponding THF solutions were subjected to investigations on their FL emission spectra. The solid TP1PBLG(*n*) films are primarily examined in Fig. 4A, which reveals that the relative emission intensity is in the order of TP1PBLG(26) > (15) > (5). The resolved emission intensity of the solid TP1PBLG(*n*)s should be correlated with the varied fractions of the α-helical structure, which will be concluded by a subsequent X-ray analysis. Similar to their solution spectra (*cf.* Fig. 2A–C), the aggregate emission band is the key leading to the emission enhancement. For AIEE-operative polymers, a higher extent of aggregate emission should also generate more intense emissions and indeed, the resultant quantum yields (Φ_Fs, Table 2) measured from the integrating sphere are 33, 41 and 60% for TP1PBLG(26), (15) and (5), respectively, which fit the qualitative view of the AIEE effect. The detrimental role of the α-helical conformation on AIEE-operative emission can be further demonstrated by the solid TP2PBLG. Here, solvent (or TFA) annealing was conducted by placing a solid TP2PBLG sample in a closed vessel saturated with THF (or TFA–THF v/v = 20/80) vapor for 10 min. As illustrated in Fig. 4B, both THF and TFA–THF vapors caused the reduction in the emission intensity; however, this intensity reduction is especially significant when treated with TFA-containing vapor. The large annealing effect of TFA should be related to its tendency to penetrate into the interior of the solid film by H-bonding to the amide linkage of the PBLG chain. Interestingly, TFA served as the FL promoter (*cf.* Fig. 2D) in the solution state of TP2PBLG but for the solid TP2PBLG sample, it functioned reversely to result in the large emission intensity reduction. The increasing fraction of the α-helical structure by TFA vapor should be the main reason leading to the intensity reduction and we will discuss this later in the X-ray diffraction study.

Table 2 The curve-fitting data from the analysis of the WAXD spectra and the resultant quantum yields of the TP1PBLG(*n*)s and TP2PBLG samples

Sample	α-Helix content[a] (%)	β-Sheet content[a] (%)	Φ_F[b] (%)
TP1PBLG(26)	90.2	9.8	33
TP1PBLG(15)	59.6	40.4	41
TP1PBLG(5)	13.9	86.1	60
Pristine TP2PBLG	75.8	24.2	21
THF-annealed TP2PBLG	76.9	23.1	17
TFA-annealed TP2PBLG	90.7	9.3	6

[a] Determined from the curve-fitting results for the WAXD peaks (*cf.* Fig. 5B and 7B) in the range of 2θ = 4–8°. [b] Determined from the integrating sphere.

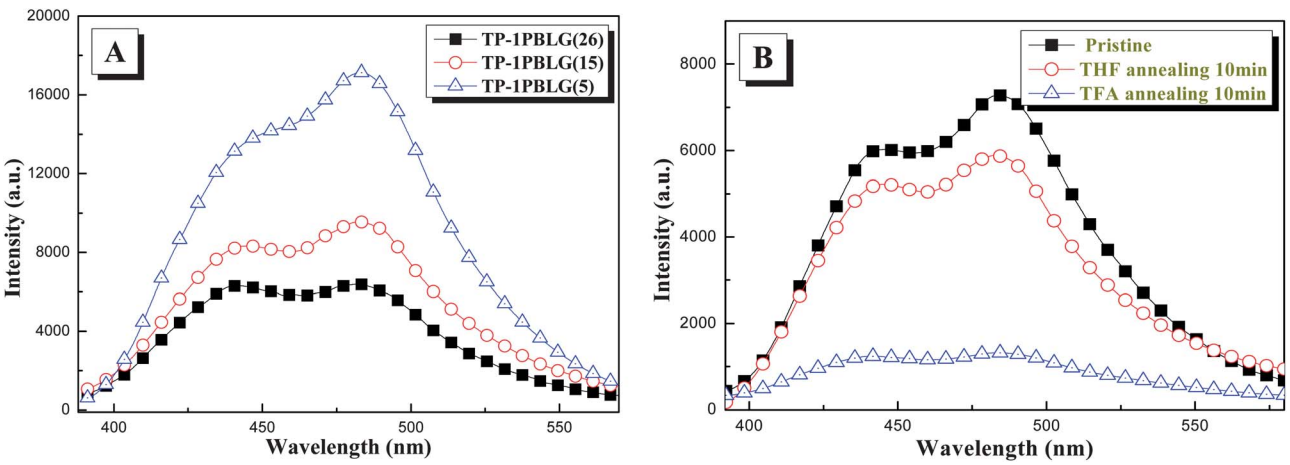

Fig. 4 The solid FL emission spectra of (A) TP1PBLG(*n*)s and (B) TP2PBLG before and after THF- and TFA-annealing.

 This journal is © The Royal Society of Chemistry 2012

Downloaded by Synchrotron Radiation Library on 21 February 2013
Published on 18 June 2012 on http://pubs.rsc.org | doi:10.1039/C2PY20221B

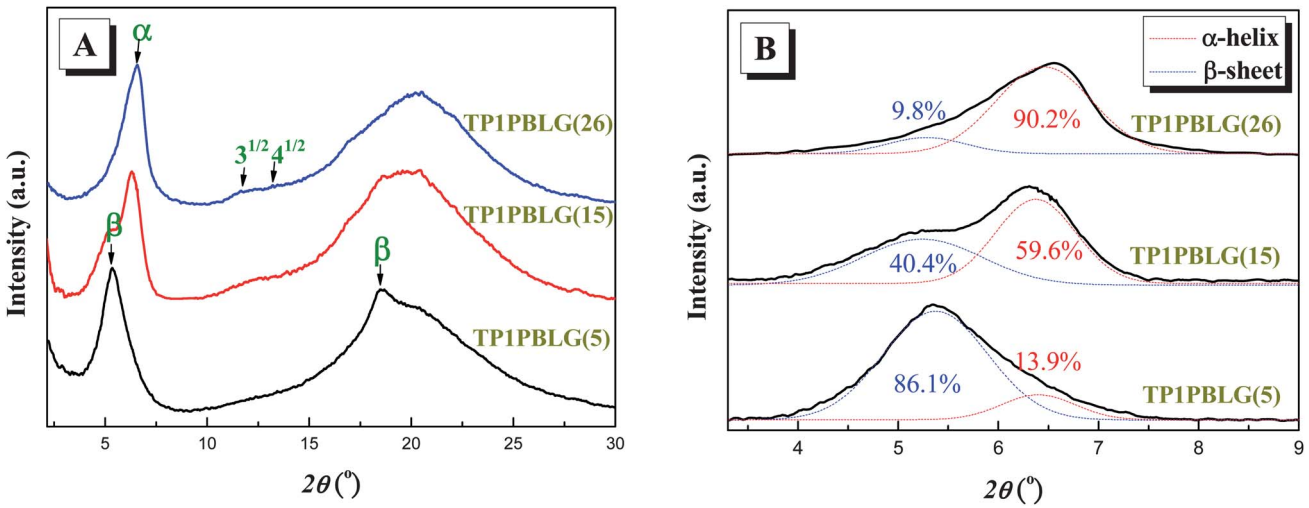

Fig. 5 (A) The WAXD diffraction pattern of TP1PBLG(*n*)s and (B) the corresponding curve-fitting results for the WAXD peaks in the range of $2\theta = 4$–$8°$.

Wide-angle X-ray diffraction (WAXD) was used to identify the secondary structure of the solid samples. As the diffraction pattern of TP1PBLG(*n*)s illustrates in Fig. 5A, the first peak at $2\theta = 5.25°$ reflects the distance ($d = 1.68$ nm) between backbones in the parallel β-pleated sheet structure and the reflection at 18.8° ($d = 0.47$ nm) represents the intermolecular distance between adjacent peptide chains with one lamella. The three reflections at higher angles, with the position $1:3^{1/2}:4^{1/2}$, relative to the primary peak at $2\theta = 6.36°$, are indexed according to the (10), (11), and (20) reflections of a 2D hexagonal packing of cylinders composed of 18/5 α-helices with a cylinder distance of 1.39 nm.[2k,l] The broad amorphous at *ca.* 20° mainly originates from the long amorphous side chain. The peaks in the range of $2\theta = 4$ to 8° were then subjected to a deconvolution process to resolve the fractions of α-helix and β-sheet structures involved in the solid samples. As summarized in Table 2, the fractions of the α-helical chain are 90.2, 59.6 and 13.9% for TP1PBLG(26), (15) and (5), respectively, which indicate the same trend reported for the alkyne-incorporated PBLGs[2l] whereby increase in molecular weight (M_w) results in the increase of the α-helical structure. Although conceivable, intermolecular approaches among the TP fluorophores vicinal to the large α-helical rods proceed more sluggishly than the TPs neighboring to the 2D β-sheet or the flexible random-coil structure. The majority of the α-helical structure in TP1PBLG(26) results in the lower emission intensity compared to those of TP1PBLG(15) and (5).

The macroscopic chain dimensions of the TP1PBLG(*n*)s can be further evaluated from the SAXS analyses (Fig. 6A). The broad peak, assumed to be a Bragg reflection, at a value of $q = 0.109$, corresponds to an ordering spacing of about 57 Å for TP1PBLG(5) while increasing the length of the PBLG chain resulted in the Bragg reflections corresponding to the spacings of 70 and 98 Å for TP1PBLG(15) ($q = 0.09$) and TP1PBLG(26) ($q = 0.064$), respectively. As illustrated in Fig. 6B, the characteristic spacing (57 Å) observed from the SAXS data is consistent with the bilayer structure of the TP1PBLG(5) in the predominant

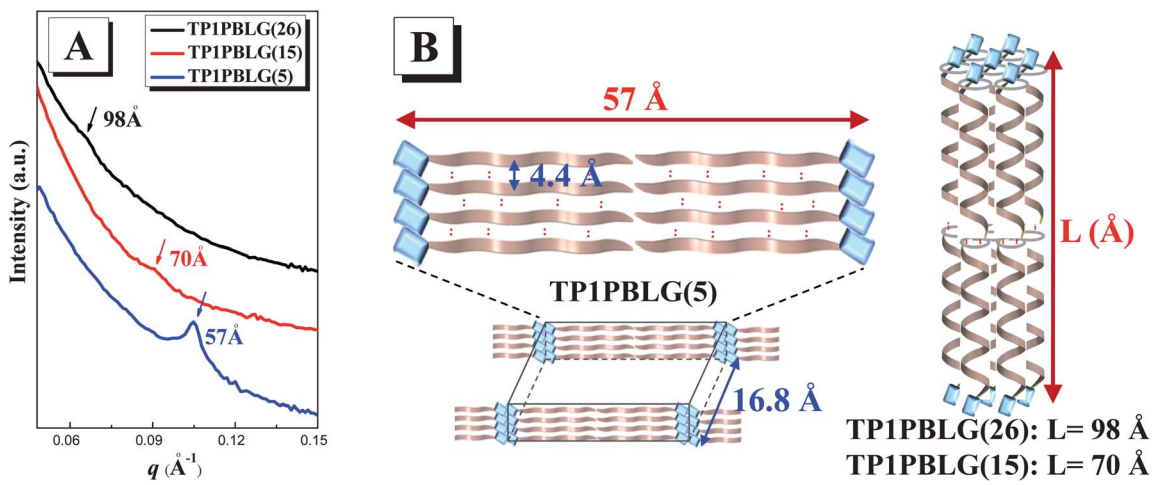

Fig. 6 (A) The SAXS diffraction pattern of TP1PBLG(*n*) and (B) the proposed model of the bilayer β-sheet structure of TP1PBLG(5) (left) and the bilayer hexagonally packed cylindrical aggregates of TP1PBLG(15) and TP1PBLG(26) (right).

Published on 18 June 2012 on http://pubs.rsc.org | doi:10.1039/C2PY20221B
Downloaded by Synchrotron Radiation Library on 21 February 2013

β-sheet (86.1%) structure as determined from WAXD (*cf.* Fig. 5A). The observed spacing of 57 Å is close to the thickness of 53 Å that is expected for the repeated packing of a "{TP}–{PBLG(5) β-sheet}–{PBLG(5) β-sheet}–{TP}" bilayer structure, as estimated from twice the sum of the TP length (2×11 Å^2) and peptide length ($2 \times 5.1 \times 3$ Å^3). For this calculation, we estimated the length of the polypeptide segment by considering the β-sheet conformation to have a length of about 3 Å for each repeat unit, rather than the length of 3.8 Å expected for fully extended peptide bonds[20] and the length of the TP unit was estimated to be about 11 Å. In addition, we would expect the observed spacing of the TP1PBLG(26) to be 98 Å (Fig. 6B, right), for the repeated packing of a "{TP}–{PBLG(26) α-helix}–{PBLG(26) α-helix}–{TP}" bilayer structure, which is close to the calculated value of 100 Å as estimated from twice the sum of the TP length (2×11 Å^2) and the peptide length ($2 \times 26/3.6 \times 5.4$ Å^3). The length of the polypeptide segment was estimated by considering the 18/5 α-helical conformations to have a length of 5.4 Å for each pitch of the helix. For TP1PBLG(15) with intermediate amounts of α-helix (59.6%) and β-sheet (40.4%), the broad band at a spacing of 70 Å is most likely due to the bilayer α-helix (Fig. 6B, right), a result that can be correlated with the calculated spacing of 68 Å (estimated from twice the TP length (2×11 Å^2) and the peptide length ($2 \times 15/3.6 \times 5.4$ Å^3)). It is reasonable to expect that the short peptide chain of TP1PBLG(15) exists in either a complete α-helical or in a complete β-sheet arrangement. The large polydispersity (PDI = 1.15) of TP1PBLG(15) was already resolved from the broad diffraction pattern for the ordered α-helix chains; therefore, it may be difficult to detect the less-ordered β-sheet structure in this case. The reduced FL emission for the annealed TP2PBLG samples is also due to the increase of the α-helical structures. As illustrated in Fig. 7A, annealing caused certain changes in the peaks in the range of $2\theta = 4$ to 8° and the de-convoluted curves in Fig. 7B indicate the increasing contents of the α-helical conformations from the pristine to the THF- and the TFA-annealed TP2PBLG samples (Table 2). During the course of annealing, the vapor molecules penetrated into the interior of the polymer film and mobilized the loosely packed chain segments (most likely, segments in coil-like or β-sheet arrangements), which in the isotropic mobile state tend to reorganize to form the stable α-helical structure during the subsequent solvent evaporation step. The increasing α-helical conformation is again the main reason leading to the decrease of FL emission intensity after vapor annealing. Notably, THF- and TFA-annealing all caused the formation of a well-defined structure corresponding to an additional sharp diffraction peak at $2\theta = 2.05°$ ($d = 43.1$ Å), which also appeared in the SAXS spectrum (inset in Fig. 7A) of the selected THF-annealed sample. The spacing of 43.1 Å is related to the geometrical arrangement of the rigid TP2PBLG chains and will be further evaluated from the 2D GIWXRDS analysis conducted subsequently.

A unidirectional shearing force was applied to a solution of TP2PBLG in THF during the sample preparative step to yield an oriented thin film for 2D WXRD analysis. The resultant 2D-GIWXRD diffraction pattern is shown in Fig. 8A, in which the X-ray beam was directed parallel to one of the two PBLG rods arranged within the hexagonally packed cylindrical aggregated domain, displaying three intense (10) reflections with 3-fold symmetry, two intense (11) reflections with 2-fold symmetry and three intense (20) reflections with 3-fold symmetry. The azimuthal angle (Fig. 8B) showed that there was a 30 degree difference between (10) and (11) reflections, which is characteristic of the two-dimensional hexagonal lattice. In addition, the higher order (11) and (20) reflections are observed at $3^{1/2}$ and 2 times the scattering vector modulus of the (10) reflection, confirming the hexagonal assignment and the spacing of (10) to be 1.39 nm (diameter of the cylindrical rod); besides the normal pattern usually observed for hexagonally packed cylindrical arrangement, two arcs positioned at 30° and 150° to the horizontal are due to the equilibrium bonding angle between the central TP unit and the two rigid α-helix chains. To theoretically approach it, $TP2NH_2$ molecule and α-helix PBLG chain were primarily constructed before energy minimization by the Molecular Studio software to obtain the stable equilibrium structures. Thereafter, $TP2NH_2$ and two α-helix PBLG chains

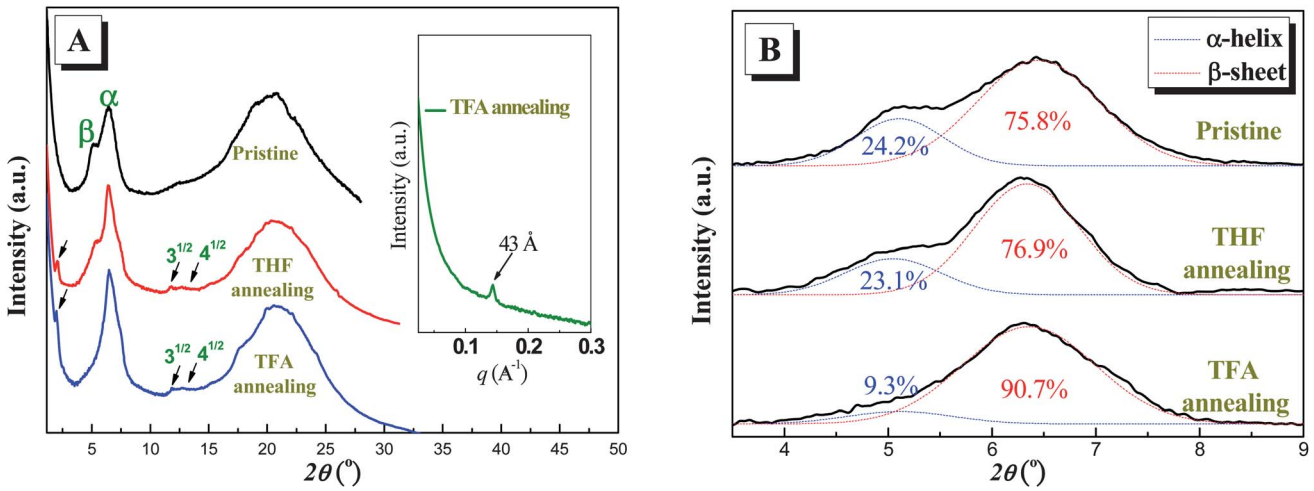

Fig. 7 (A) The WAXD diffraction pattern of TP1PBLG(*n*)s and (B) the corresponding curve-fitting results for the WAXD peaks in the range of $2\theta = 4$–8°.

 This journal is © The Royal Society of Chemistry 2012

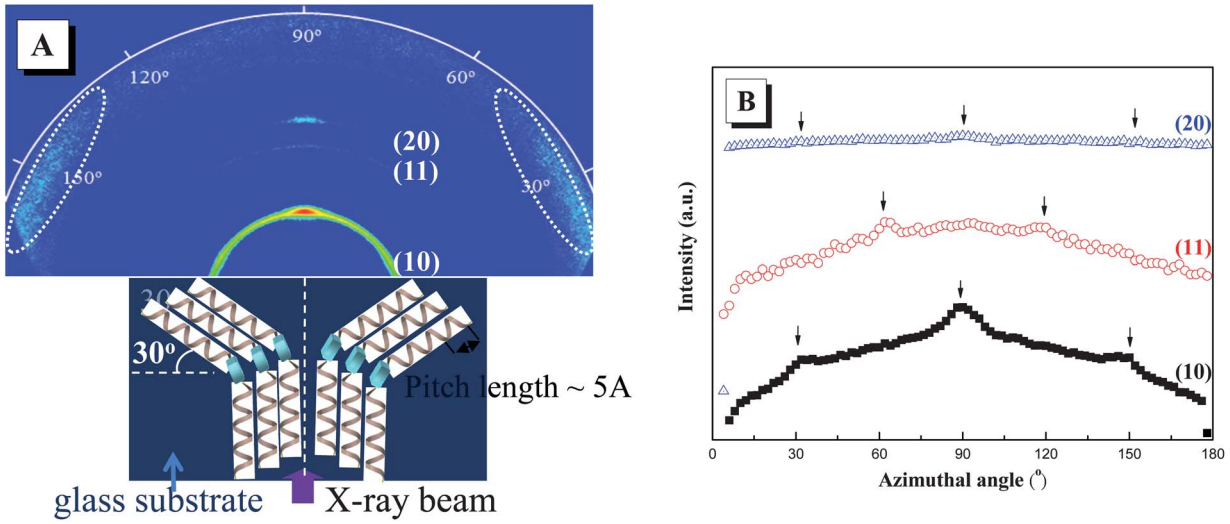

Fig. 8 (A) 2D-GIWAXD pattern of the aligned TP2PBLG thin film (upper), schematic diagram showing the relative direction between the incident X-ray and the cylindrical aggregates of the TP2PBLG sample, with the oriented cylindrical aggregates within the TP2PBLG sample aligned parallel to the incident X-rays; (B) azimuthal scans of the 2D-GIWAXD pattern in (A) from 0° to 180°.

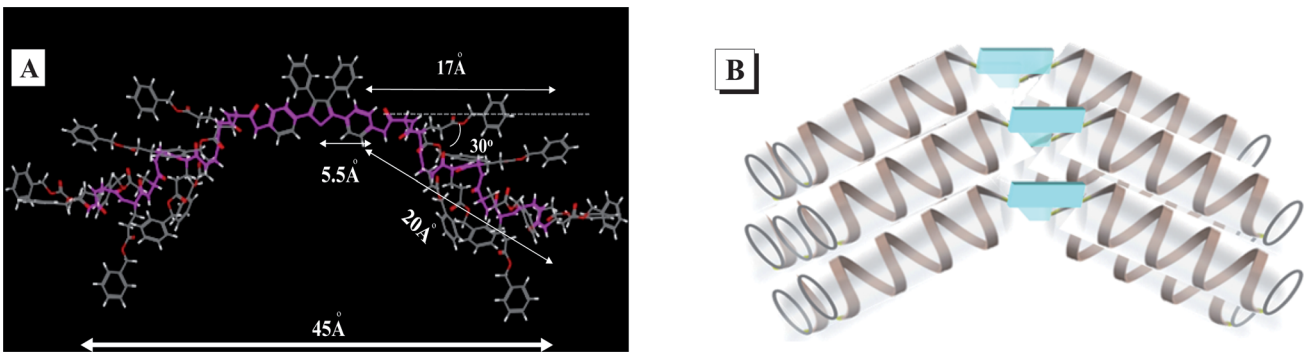

Fig. 9 The simulated single chain conformation of TP2PBLG (left) from the Molecular Studio software and the schematic illustration of the hexagonally packed bent-core cylinder aggregates (right).

Published on 18 June 2012 on http://pubs.rsc.org | doi:10.1039/C2PY20221B
Downloaded by Synchrotron Radiation Library on 21 February 2013

were manually linked together to build up the prototype TP2PBLG model. After energy minimization, the single chain conformer of TP2PBLG actually adopts the bent-core geometry (Fig. 9A), in which the two α-helical chains are bonded to the central TP core with a bent angle of 30°. The calculated molecular length of 45 Å here is correlated with the experimental result of 43.1 Å. The bent cylindrical rods therefore self-assemble into hexagonal arrays (Fig. 9B).

Comparison between TP1PBLG(*n*)s and TP2PBLG

According to Scheme 1, irrespective of whether the linking PBLG chain is in α-helix or β-sheet or random-coil conformation, the TP terminals in TP1PBLG(*n*)s are spatially accessible to each other. In fact, the bilayer α-helix and β-sheet arrangements (*cf.* Fig. 6B) all permit the intermolecular contacts between two terminal TPs. In contrast, mutual approaches among the central TP cores of the TP2PBLG are sterically prohibited when the TP unit is tethered to the large α-helical PBLG chains (*cf.* Fig. 9B). The blocking effect of the α-helical chain in TP2PBLG can be experimentally evidenced by the relationship between the fraction of the secondary structure and the resolved Φ_F values are summarized in Table 2. Despite its lower α-helix content (75.8 *vs.* 90.2%), the pristine TP2PBLG film actually emits with a lower Φ_F value than TP1PBLG(26) (21 *vs.* 33%). This effect can be also emphasized by comparison of the results from the TP1PBLG(26) and the TFA-annealed TP2PBLG films, that is, with comparable α-helix content (90.7 *vs.* 90.2%), TFA-annealed TP2PBLG emitted with much lower Φ_F value than TP1PBLG(26) (6 *vs.* 33%). The two vicinal PBLG chains of TP2PBLG are therefore efficient in blocking the inherent TP fluorophores from contacting each other, thus, deactivating the AIEE-operative emission to result in low emission intensity. The high content of the TP fluorophore and the low fraction of the α-helical chain in TP1PBLG(5) contribute to its high Φ_F value of 60%.

Conclusions

Three TP1PBLG(*n*) and one TP2PBLG copolymers were prepared by ring opening polymerizations (ROP) of the BLG-NCA monomer initiated by $TPNH_2$ and $TPNH_2$, respectively.

Published on 18 June 2012 on http://pubs.rsc.org | doi:10.1039/C2PY20221B
Downloaded by Synchrotron Radiation Library on 21 February 2013

All the MW values determined from the ^{1}H NMR and MALDI-TOF spectra correlate well.

The resultant TP1PBLG(*n*)s showed typical AIEE features with increasing emission intensity with increasing water content in the solutions. In contrast, aggregation resulted in little emission enhancement for the TP2PBLG system, which suggests that intermolecular approaches of the central TP units of TP2PBLG are retarded by the neighboring PBLG chain in the large α-helical conformation. However, helix–coil transition induced by the TFA additive resulted in the emission enhancement with the facile aggregation of TP fluorophores bisected by coil-like PBLG chains.

The emission of the solid films was also related to the relative fractions of the large α-helical secondary structure. Primarily, TP fluorophores in the di-substituted TP2PBLG are more severely isolated by the vicinal α-helix PBLG rod, leading to the reduced AIEE-operative emission, than TP in the mono-substituted TP1PBLG(*n*)s. Secondly, increasing chain length of TP1PBLG(*n*)s results in the increase of the α-helical rod, which contributes to the reduced emission intensity in the order of TP1PBLG(5) > (15) > (27). Thirdly, solvent or TFA annealing causes the increase of the α-helical rod, which also contributes to the reduced emission of the TP2PBLG film.

The WXRD and SXRD study evaluated the fundamental chain conformations of TP1PBLG(*n*)s and TP2PBLG. The self-assembled bilayer β-sheet and the α-helix rod in the bilayer hexagonal cylindrical packing were both found in TP1PBLG(*n*)s but with the predominant β-sheet conformation of TP1PBLG(5) gradually transforming into the major α-helical conformation by the increase of chain length from TP1PBLG(15) to TP1PBLG(26). For TP2PBLG, the bent-core connected by two cylindrical rods was found to self-assemble into the dense hexagonal packing, which resulted in its low emission intensity due to the efficient blocking effect of the two large α-helix rods.

Acknowledgements

We appreciate the ingenious work from National Synchrotron Radiation Research Center (NSRRC) on the 2D-GIWAXD analysis and the financial support from National Science Council, Taiwan under contract no. NSC-100-2221-E-110-045.

Notes and references

1 (*a*) Y. Bae, S. Fukushima, A. Harada and K. Kataoka, *Angew. Chem., Int. Ed.*, 2003, **42**, 4640–4643; (*b*) H. A. Klok and S. Lecommandoux, *Adv. Mater.*, 2001, **13**, 1217–1229; (*c*) H. Tang and D. Zhang, *J. Polym. Sci., Part A: Polym. Chem.*, 2010, **48**, 2340–2350; (*d*) G. J. M. Habraken, C. E. Koning and A. Heise, *J. Polym. Sci., Part A: Polym. Chem.*, 2009, **47**, 6883–6893; (*e*) P. J. Flory, *Proc. R. Soc. London, Ser. A*, 1956, **234**, 73–89; (*f*) C. Robinson and J. C. Ward, *Nature*, 1957, **180**, 1183–1184; (*g*) S. M. Yu, V. P. Conticello, G. Zhang, C. Kayser, M. J. Fournier, T. L. Mason and D. A. Tirrell, *Nature*, 1997, **389**, 167–170; (*h*) K. Tohyama and W. G. Miller, *Nature*, 1981, **289**, 813–814; (*i*) S. W. Kuo, H. F. Lee and F. C. Chang, *J. Polym. Sci., Part A: Polym. Chem.*, 2008, **46**, 3108–3119; (*j*) A. Gitsas, G. Floudas, M. Mondeshki, H. W. Spiess, T. Aliferis, H. Iatrou and N. Hadjichristidis, *Macromolecules*, 2008, **41**, 8072–8080.

2 (*a*) T. Torii, T. Yamashita and K. Horie, *Eur. Polym. J.*, 1993, **29**, 1265–1270; (*b*) P. Doty, J. H. Bradbury and A. M. Holtzer, *J. Am. Chem. Soc.*, 1956, **78**, 947–954; (*c*) F. A. Bovey and G. V. D. Tiers, *Adv. Polym. Sci.*, 1963, **3**, 139–195; (*d*) R. H. Wieringa, E. A. Siesling, P. J. Werkman, H. J. Angerman, E. J. Vorenkamp and A. J. Schouten, *Langmuir*, 2001, **17**, 6485–6490; (*e*) A. J. Wada, *J. Polym. Sci.*, 1960, **45**, 145–153; (*f*) M. Gregson, G. P. Jones and M. Davies, *Chem. Phys. Lett.*, 1970, **6**, 215–216; (*g*) A. K. Gupta, C. Dufour and E. Marchal, *Biopolymers*, 1974, **13**, 1293–1308; (*h*) V. Pokorná, D. Výprachtický and J. Pecka, *Macromol. Biosci.*, 2001, **1**, 185–190; (*i*) K. T. Kim, C. Park, G. W. M. Vandermeulen, D. A. Rider, C. Kim, M. A. Winnik and I. Manners, *Angew. Chem.*, 2005, **117**, 8178–8182; (*j*) L. Rubatat, X. Kong, S. A. Jenekhe, J. Ruokolainen, M. Hojeij and R. Mezzenga, *Macromolecules*, 2008, **41**, 1846–1852; (*k*) P. Papadopoulous, G. Floudas, H. A. Klok, I. Schnell and T. Pakula, *Biomacromolecules*, 2004, **5**, 81–91; (*l*) Y. C. Lin and S. W. Kuo, *J. Polym. Sci., Part A: Polym. Chem.*, 2011, **49**, 2127–2137; (*m*) A. Sanchez-Ferrer and R. Mezzenga, *Macromolecules*, 2010, **43**, 1093–1100; (*n*) J. Lin, N. Liu, J. Chen and D. Zhou, *Polymer*, 2000, **41**, 6189–6194; (*o*) D. Voet and J. G. Voet, *Biochemistry*, Hoboken, NJ, Wiley, 2004; p. 227.

3 (*a*) J. Z. Xie, J. W. Y. Lam, L. Cheng, H. Chen, C. Qiu, H. S. Kwok, X. Zhan, Y. Liu, D. Zhu and B. Z. Tang, *Chem. Commun.*, 2001, 1740–1741; (*b*) C. X. Yuan, X. T. Tao, L. Wang, J. X. Yang and M. H. Jiang, *J. Phys. Chem. C*, 2009, **113**, 6809–6814; (*c*) Z. Yang, Z. Chi, T. Yu, X. Zhang, M. Chen, B. Xu, S. Liu, Y. Zhang and J. Xu, *J. Mater. Chem.*, 2009, **19**, 5541–5546; (*d*) W. Z. Yuan, P. Lu, S. Chen, J. W. Y. Lam, Z. Wang, Y. Liu, H. S. Kwok, Y. Ma and B. Z. Tang, *Adv. Mater.*, 2010, **22**, 1–5; (*e*) B. Xu, Z. Chi, Z. Yang, J. Chen, S. Deng, H. Li, X. Li, Y. Zhang, N. Xu and J. Xu, *J. Mater. Chem.*, 2010, **20**, 4135–4141; (*f*) Z. Zhao, S. Chen, J. W. Y. Lam, P. Lu, Y. Zhong, K. S. Wong, H. S. Kwok and B. Z. Tang, *Chem. Commun.*, 2010, **46**, 2221–2223; (*g*) J. Liu, J. W. Y. Lam and B. Z. Tang, *J. Inorg. Organomet. Polym. Mater.*, 2009, **19**, 249–285; (*h*) J. Liu, Y. Zhong, J. W. Y. Lam, P. Lu, Y. Hong, Y. Yu, Y. Yue, M. Faisal, H. H. Y. Sung, I. D. Williams, K. S. Wong and B. Z. Tang, *Macromolecules*, 2010, **43**, 4921–4936; (*i*) R. H. Chien, C. T. Lai and J. L. Hong, *J. Phys. Chem. C*, 2011, **115**, 5958–5965; (*j*) C. T. Lai and J. L. Hong, *J. Phys. Chem. B*, 2010, **114**, 10302–10310; (*k*) C. T. Lai, R. H. Chien, S. W. Kuo and J. L. Hong, *Macromolecules*, 2011, **44**, 6546–6556; (*l*) R. H. Chien, C. T. Lai and J. L. Hong, *Macromol. Chem. Phys.*, 2012, **213**, 666–677.

4 W. H. Daly and D. Poche, *Tetrahedron Lett.*, 1988, **29**, 5859–5862.

 This journal is © The Royal Society of Chemistry 2012